Directing the Assembly of Gold Nanoparticles with Two-Dimensional Molecular Networks

Mohamed A. Mezour, Iryna I. Perepichka, Jun Zhu, R. Bruce Lennox,* and Dmitrii F. Perepichka*

Department of Chemistry and Centre for Self-Assembled Chemical Structures, McGill University, 801 Sherbrooke Street West, Montreal (QC) H3A 0B8, Canada

ABSTRACT Lamellar patterns resulting from the adsorption of *p*-dialkoxybenzene derivatives on HOPG have been investigated as molecular templates for directing the assembly of thiol-capped gold nanoparticles (AuNP). STM characterization at the liquid–solid interface reveals the periodic arrangement of AuNP on top of the self-assembled molecular network (SAMN), spanning hundreds of nanometers. The resulting superlattices are notably different from the close-packed structures formed by spherical nanoparticles during evaporative drying. The templating effect is based on van der Waals interactions of the alkyl chains of the SAMN and AuNP, and the assembly efficiency is greatest when these chains are of similar length.

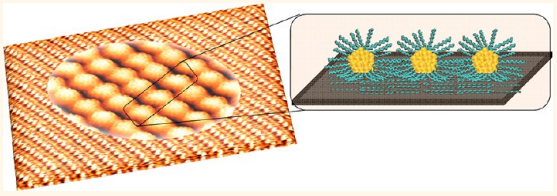

KEYWORDS: surface nanopatterning · molecular template · self-assembled molecular network · gold nanoparticles · scanning tunneling microscopy

The precise organization of nano-objects into well-defined patterns at surfaces and interfaces offers a versatile approach to the development of technologically important materials and devices.[1] Among the various existing nanopatterning methods,[2,3] self-assembly has gained increasing attention as a highly accurate, efficient, and low-cost "bottom-up" approach.[4–6] Molecular self-assembly in particular provides a flexible and efficient way to create complex structures and patterns with subnanometer precision over an extended length scale.[7,8] Using supramolecular chemistry "tools" (*i.e.*, hydrogen bonding, van der Waals (vdW) interactions, π–π stacking, metal coordination), self-assembled molecular networks (SAMNs) with a broad variety of architectures have been developed and explored as molecular templates. For example, SAMNs of porous, lamellar, and polymeric nanostructures have been reported to template various molecular guests, such as fullerenes,[9–11] flat polyaromatic hydrocarbons,[12–14] and other large macrocyclic molecules.[15–17]

Nanoparticles (NPs) can exhibit a range of desirable electronic, magnetic, and optical properties, and thus their templated assembly is of particular interest.[18,19] Various routes to direct NP self-assembly have been explored, including Langmuir–Blodgett deposition,[20] interfacial assembly,[21] and droplet evaporation.[22] However in most cases, organization of NPs is restricted to the formation of centrosymmetric close-packed lattices, as the particle–particle interactions dominate particle–substrate interactions. Structurally complex arrays of NP can be obtained employing macromolecules as templates including DNA,[23] linear polymers,[24] and block copolymers.[25,26] While remarkable and oftentimes useful, these templates are synthetically complex, and the resulting NP arrays are limited in size (as in DNA-driven assemblies) or in long-range order (as in block-copolymer-driven assemblies). In this context, the high reproducibility, versatility, and precision offered by SAMNs make them an intriguing means for templating nanoparticle assemblies with tunable periodicity and long-range order.

Little however is known about NP assembly on SAMNs. To our knowledge, the reported studies are limited to (i) AuNP assembly on fatty acid SAMNs,[27] (ii) NiNP assembly on long alkane and alkylthiol SAMNs on HOPG[28] (both attributed to vdW interactions), and (iii) AuNP assembly on a dialkoxyanthracene derivative SAMN modified with –COOH functional groups using ionic interactions with Cu^{2+}.[29] Although the existing reports demonstrate the viability of NP adsorption on a SAMN

* Address correspondence to dmitrii.perepichka@mcgill.ca; bruce.lennox@mcgill.ca.

Received for review October 14, 2013 and accepted February 10, 2014.

Published online February 10, 2014
10.1021/nn405357j

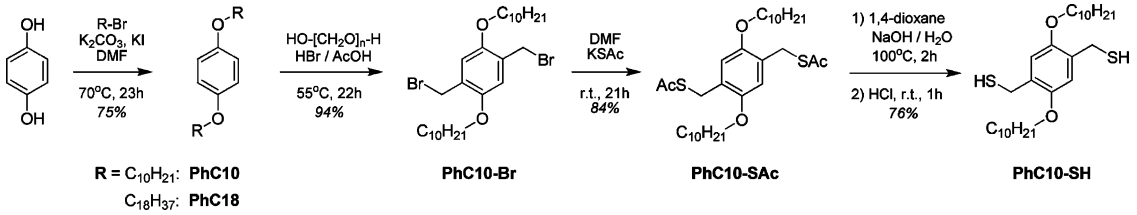

Scheme 1. Synthesis of template-forming molecules.

template, little to no long-range order and very limited coverage has been achieved to date.

Herein, we explored the use of simple *p*-dialkoxybenzene derivatives as templates for directing the two-dimensional assembly of thiol-capped AuNPs from solution. Using scanning tunneling microscopy (STM) at a solid–liquid interface, we show that AuNPs assemble on lamellar SAMNs to create long-range order 2D structures whose periodicities and lattice directions are commensurate with those of the SAMN template. The aforementioned assembly is driven by vdW interactions between the alkyl chains on the AuNP surface and in SAMNs, and the efficiency of assembly is highest when the alkyl chains of each are of similar lengths.

RESULTS

Self-Assembly of Molecular Network. Our design of molecular building blocks was based on the requirements of predictable long-range self-assembly, the possibility for tuning the periodicity of the resulting molecular template, and a provision for specific interactions with nanoparticles. *p*-Dialkoxybenzene derivatives are among the simplest and most synthetically versatile compounds fulfilling these requirements (Scheme 1). Two alkoxy chains provide strong vdW stabilization of the 2D molecular pattern at an HOPG surface.[30−32] The periodicity of such a pattern can be controlled by the length of the alkyl groups (decyl *vs* octadecyl). The aromatic core enables facile introduction of various functionalities, such as thiol sites for potential binding to AuNPs (while the use of free dithiols in air is problematic due to oxidative polymerization, acetyl-protected thiols have also been shown to form RS-Au bonds).[33]

Deposition of 1,4-di(decyloxy)-2,5-bis(*S*-acetylthiomethyl)benzene (PhC10-SAc) from a tetradecane solution onto the HOPG surface results in the spontaneous formation of a stable monolayer of PhC10-SAc molecules. Within a few minutes after deposition, STM imaging at the solid–liquid interface reveals that the surface is covered with a lamellar structure of alternating bright and dark stripes. These correspond to the aromatic core and alkyl chains, respectively, in accord with previous observations in similar SAMNs (Figure 1).[30−32]

The SAMN contains one molecule per unit cell (a = 2.1 ± 0.1 nm, b = 1.0 ± 0.1 nm, and α = 86 ± 1°, plane group *p*2), with the lamellae width (2.1 ± 0.1 nm) defined by fully extended and interdigitated decyloxy substituents. This packing, frequently reported

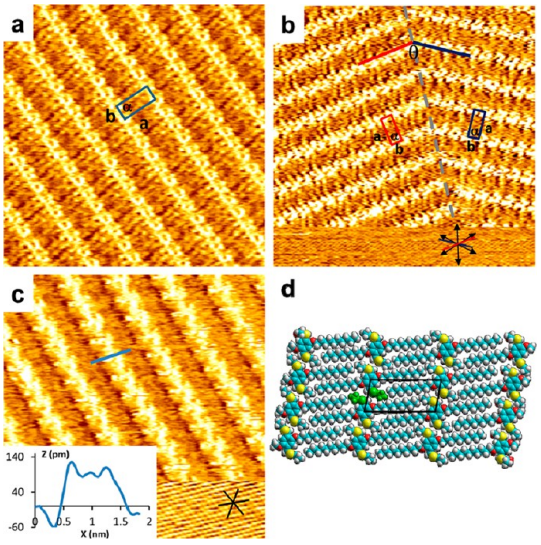

Figure 1. (a) Representative STM image (14 × 14 nm^2; V_b = 700 mV, I_t = 0.2 nA) of PhC10-SAc showing the unit cell: a = 2.1 ± 0.1 nm; b = 1.0 ± 0.1 nm, α = 86 ± 1°. (b) STM image (21 × 21 nm^2) showing two domains of PhC10-SAc (V_b = 1373 mV, I_t = 0.2 nA) simultaneously resolved with the underlying HOPG (V_b = 50 mV, I_t = 0.2 nA). The black arrows indicate the main crystallographic axes of graphite ⟨−1100⟩. The red and blue lines indicate the lamellar directions. (c) Smaller scale STM image (12 × 12 nm^2; V_b = 700 mV, I_t = 0.09 nA (for SAMN) and V_b = 25 mV, I_t = 0.09 nA for HOPG) reveals out-of-plane substituents in the benzene ring (inset: cross-sectional profile corresponding to blue line). (d) Molecular mechanics model of the 2D packing of PhC10-SAc on a graphene sheet; optimized unit cell parameters: a = 2.1 nm; b = 0.93 nm, α = 81°. The green color identifies the upright position of the acetylthiol group.

for the assembly of alkylated aromatic molecules on HOPG,[30−32] is driven mainly by the attractive lateral interaction between alkoxy chains and the in-registry adsorption of alkoxy chains along one of the principal axes of the HOPG lattice.

Larger scale images reveal that the adjacent domains within the PhC10-SAc monolayer are always oriented at an angle of θ = 148 ± 3° with respect to one another (Figure 1b and Figure SI1). Such an orientational effect is generally associated with co-alignment of alkyl chains of neighboring domains and a chiral unit cell. It can be used to deduce the angle γ between the alkyl chains and the direction of the lamellae (unit cell axis b): $\gamma = \theta/2 = 74 \pm 2°$ (see Figure SI2). Simultaneous imaging of the SAMN and the underlying HOPG lattice (Figure 1b,c) demonstrates an epitaxial relationship between the two. The lamellae

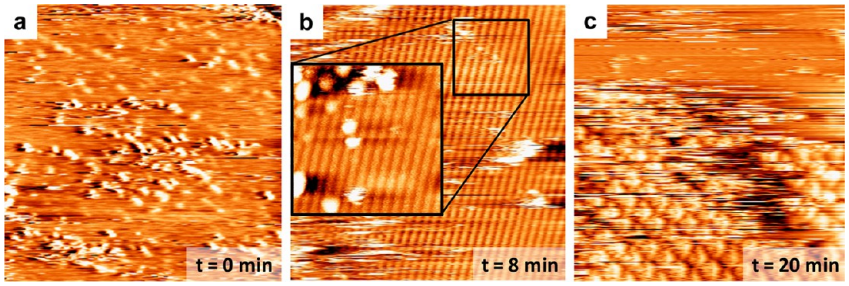

Figure 2. STM images of AuNP-C12SH assembly on top of HOPG before and after adding PhC10-SAc. (a) Representative STM image (130 × 130 nm^2; V_b = 800 mV, I_t = 0.1 nA) of AuNP-C12SH at tetradecane/HOPG. (b, c) STM images (80 × 80 nm^2 and 50 × 50 nm^2; V_b = 800 mV, I_t = 0.08 nA) of AuNPs at the tetradecane/PhC10-SAc/HOPG interface after 8 and 20 min of time scanning, respectively.

of PhC10-SAc SAMN are oriented with respect to the nearest main crystallographic axis of HOPG, at angles of 14 ± 2° (Figure 1b). These angles originate from the above-mentioned tilt γ of the alkyl chains (14° = 74°−60°).

The aromatic cores in PhC10-SAc SAMN were not well resolved. The fuzzy image of the aromatic cores can be attributed to the conformational freedom of the thioacetyl groups, which protrude out of the plane of the monolayer. This behavior was previously reported for molecules bearing out-of-plane substituents.[34] At certain tunneling conditions, it was possible to resolve pairs of bright spots on the sides of bright lamellae (Figure 1c). Their location and spacing (~0.75 nm) are in good agreement with the position of the acetyl groups predicted by the molecular model (Figure 1d). The calculated unit cell parameters (a = 2.1 nm; b = 0.93 nm, α = 81°) are in reasonable agreement with the experimental values.

A similar SAMN could also be prepared with the deprotected dithiols PhC10-SH (Figure SI3). However, the spacing of molecules along the lamellae is less uniform and the STM imaging is more difficult to reproduce, suggesting an occurrence of the anticipated oxidative cross-linking of the thiol groups (*via* disulfide bridge).

Assembly of AuNP on PhC10-SAc-Modified HOPG. In order to explore the potential of SAMN to template the assembly of nanomaterials, gold nanoparticles (AuNPs) stabilized by a dodecanethiol ligand shell (C12SH) were synthesized by the Brust−Schiffrin method.[35] The nanoparticles were purified by repeated (10×) washing with ethanol to remove the excess free thiol ligand and the quaternary ammonium salt (used as the phase transfer reagent), dried in vacuum, and redissolved in tetradecane for the STM investigation at the liquid−solid interface. The template-directed assembly of AuNP was carried out on samples with a typical mean size of 1.9 ± 0.3 nm (Figure SI4). The size distribution of nanoparticles is known to be critical for their self-assembly into ordered arrays.[36] Indeed, higher polydispersity AuNP samples (3 ± 1 nm) were not successful in the self-assembly experiments described below (Figure SI5).

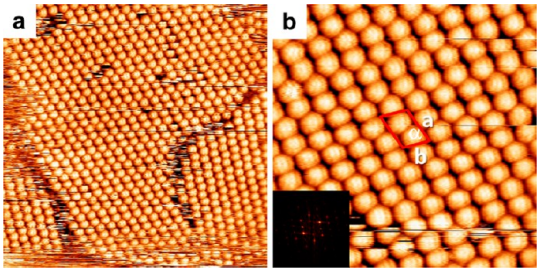

Figure 3. (a) Large-scale and (b) high-resolution STM images (100 × 100 nm^2 and 40 × 40 nm^2; V_b = 700 mV, I_t = 0.1 nA) of AuNP-C12SH at the tetradecane/PhC10-SAc-modified HOPG interface. Unit cell parameters: a = 6.1 ± 0.2 nm, b = 4.1 ± 0.1 nm, α = 67 ± 2°. Inset: FFT of image (b).

Adsorption of thiol-capped AuNPs on top of bare HOPG using a simple immersion procedure was reported to lead to inhomogeneous, disordered aggregates.[37,38] Our control experiments involving deposition of tetradecane solutions of AuNP onto HOPG did not lead to any self-assembly, and only scattered, disordered aggregates of nanoparticles were observed (Figure 2a). However, within a few minutes after adding PhC10-SAc, the characteristic periodic lamellar structure of PhC10-SAc was formed (Figure 2b). This was shortly followed by the appearance of small domains of bright protrusions attributable to ordered AuNP assemblies (Figure 2c). Higher quality STM images were typically obtained by adding AuNP after the complete formation of PhC10-SAc SAMN.

Within *ca.* 20 min after placing a drop of saturated tetradecane solution of AuNP onto the PhC10-SAc-modified HOPG, large domains of the AuNP superlattice are clearly observed with STM (Figure 3). Individual AuNPs are resolved as bright circular protrusions arranged in a 2D periodic lattice with an oblique unit cell (a = 6.1 ± 0.2 nm, b = 4.1 ± 0.1 nm, α = 67 ± 2°) that contains two nanoparticles. The observed unit cell is distinctly different from the close-packed arrangements of spherical particles that form a hexagonal lattice on surfaces.[39,40] Note that the size uniformity of the assembled AuNP arrays displayed in the STM images (Figure 3) is substantially better than that of the entire AuNP sample as assessed by TEM (Figure SI4).

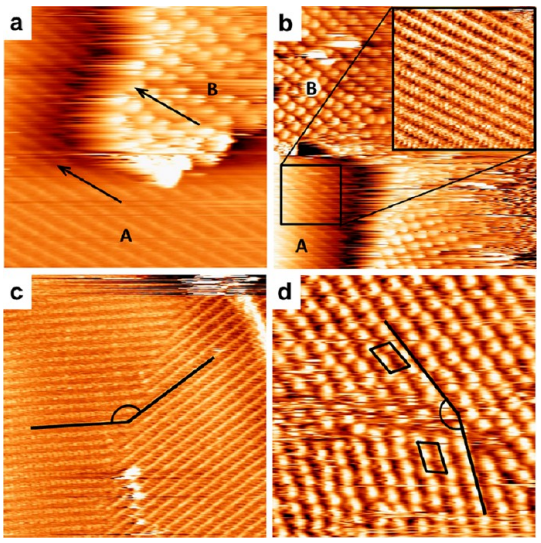

Figure 4. (a, b) STM images (*a*: 60 × 60 nm^2, V_b = 800 mV, I_t = 0.1 nA; *b*: 50 × 50 nm^2, V_b = 800 mV, I_t = 0.3 nA) showing domains of PhC10-SAc (region A) and AuNP-C12SH (region B) simultaneously. The inset in (b) corresponds to a (29 × 29 nm^2) zoom of the molecular network of PhC10-SAc. The black arrows in (a) indicate a parallel orientation of the PhC10-SAc lamellae and AuNP rows. (c) STM image (52 × 52 nm^2; V_b = 800 mV, I_t = 0.1 nA) of PhC10-SAc domains oriented at 148 ± 3°. (d) STM image (80 × 80 nm^2; V_b = 800 mV, I_t = 0.09 nA) of AuNP domains oriented at 154 ± 4°.

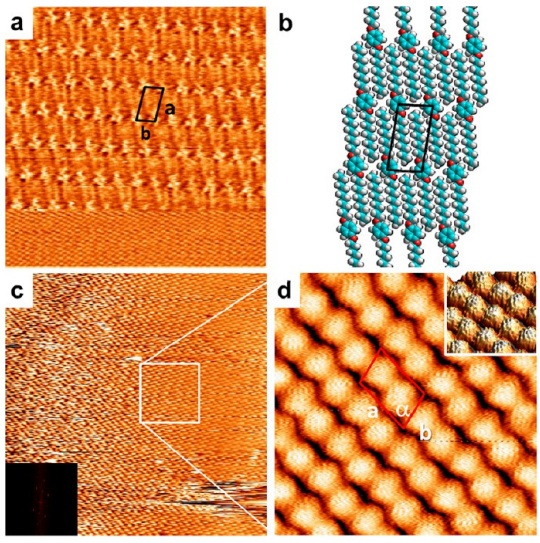

Figure 5. (a) Typical high-resolution STM image (13.7 × 13.7 nm^2) simultaneously showing the SAMN of PhC10 molecules (V_b = 500 mV, I_t = 0.2 nA) and the underneath HOPG lattice (V_b = 50 mV, I_t = 0.2 nA). Unit cell parameters: *a* = 1.8 ± 0.2 nm, *b* = 1.00 ± 0.1 nm, α = 80 ± 2°. (b) Molecular mechanics model of the 2D packing of PhC10 on a graphene sheet, with optimized unit cell parameters: *a* = 1.78 nm, *b* = 0.91 nm, α = 83°. (c) Large-scale STM image (72.5 × 72.5 nm^2, V_b = 500 mV, I_t = 0.1 nA) of AuNP at the tetradecane/PhC10-modified HOPG interface. Inset: Corresponding FFT image. (d) High-resolution STM image (25 × 25 nm^2, V_b = 500 mV, I_t = 0.1 nA) showing rows of well-aligned AuNP-C12SH. Unit cell parameters: *a* = 6.1 ± 0.2 nm, *b* = 3.9 ± 0.1 nm, α = 73 ± 2°. Inset: 3D image of AuNP assembly showing the protrusions on AuNP.

This highlights the role of the dynamic equilibrium at the solid−liquid interface in selecting nanoparticles of optimal size during the self-assembly process.

Simultaneous imaging of the molecular network and the AuNP superlattice gives additional insight into the templating effect of the SAMN in directing the AuNP assembly (Figure 4a,b). The STM images reveal coalignment of the close-packed axis of the AuNP domain with the lamellae axis of the PhC10-SAc SAMN (marked by black arrows in Figure 4a), which highlights the template/overlayer relationships between them. This templating effect is also supported by the agreement (within experimental error) of the angles between the domain of the AuNP assembly (154 ± 4°) and the domains of the PhC10-SAc SAMN (148 ± 3°).

From the above experiments we conclude that the PhC10-SAc molecular adlayer acts as a sticky template and that the structural information of the underlying monolayer is transferred to the AuNP assembly.

Self-Assembly of AuNP on Nonthiolated PhC10 SAMN. The thiol functionality of Ph10-SAc was initially viewed to be a means to "graft" the AuNP to the SAMN. It was therefore important to verify whether the presence of thioacetyl groups in the template structure is essential for directing AuNP self-assembly. For this purpose, we repeated the experiments with PhC10, which produces a similar SAMN but lacks thiol substituents.

Deposition of a tetradecane solution of PhC10 onto HOPG (Figure 5a) leads to a slightly narrower lamellar structure compared to that of PhC10-SAc (Figure 5c), consistent with the absence of AcS substituents. The unit cell parameters are *a* = 1.8 ± 0.1 nm, *b* = 1.00 ± 0.1 nm, and α = 80 ± 1°. Addition of a tetradecane solution of AuNP-C12SH on top of this SAMN creates well-ordered domains of AuNP spanning many hundreds of nanometers (Figure SI7). High-resolution STM images (Figure 5d) allow for identification of rows of the aligned AuNP and measurement of the unit cell (*a* = 6.1 ± 0.2 nm, *b* = 3.9 ± 0.1 nm, α = 73 ± 2°). This unit cell is only slightly smaller than that obtained on the PhC10-SAc template; the difference is at the edge of the uncertainty range of the measurements (see the SI) but is expected based on periodicities of the two SAMNs. On the other hand, the fact that similar AuNP superlattices were obtained on both PhC10-SAc and PhC10 templates strongly suggests that the self-assembly of AuNP is driven by vdW interactions between the alkyl chains of the AuNP and the molecular template.

It is interesting to note that such immobilization of AuNP on the SAMN-modified surface enables facile STM resolution of fine features on the AuNP surface (Figure 5d). These dots form ripples that are separated by ~0.6 nm, a value close to the expected distance between the terminal CH_3 groups of the ligands (see Figure SI9 for images with other scanning directions and speed). Similar features were observed

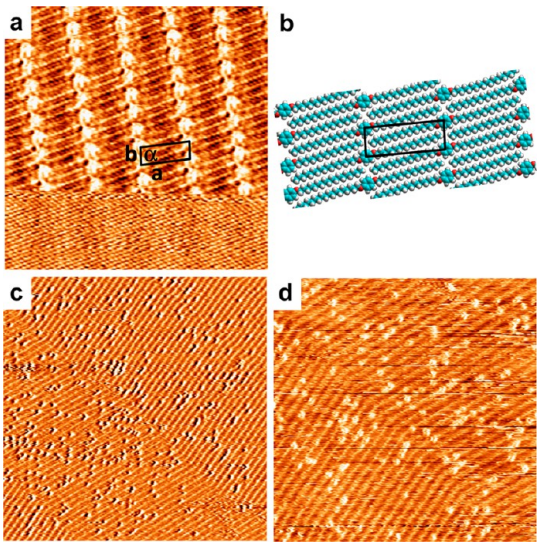

Figure 6. (a) High-resolution STM image (14.5 × 14.5 nm^2) showing the SAMN of PhC18 molecules (V_b = 700 mV, I_t = 0.25 nA) and the underneath HOPG lattice (V_b = 50 mV, I_t = 0.25 nA) simultaneously. Unit cell parameters: a = 2.7 ± 0.1 nm, b = 1.0 ± 0.1 nm, α = 85 ± 2°. (b) Molecular mechanics model for the 2D packing of PhC18 on a graphene sheet, with optimized unit cell parameters: a = 2.72 nm, b = 0.93 nm, α = 87°. (c, d) STM images (c: 200 × 200 nm^2; V_b = 900 mV, I_t = 0.1 nA; d: 93.5 × 93.5 nm^2; V_b = 1000 mV, I_t = 0.5 nA) of AuNP at the tetradecane/PhC10-SAc-modified HOPG interface.

by Stellacci and co-workers for thiol-protected AuNP immobilized on nonpatterned surfaces,[41] but only when two dissimilar, presumably phase-separated, thiols were used (octanethiol-protected AuNP also showed dots separated by ~0.6 nm,[42] but no ripples). The nature of these ripples has been debated in the literature,[43,44] and, while it is outside the scope of this paper, we hope that our observations may shed further light on this question.

Self-Assembly of AuNP on PhC18 SAMN. The length of the alkoxy substituents in the molecular template was extended in order to explore the possible control over the spacing of AuNPs. Similar to PhC10 and PhC10-SAc, 1,4-bis(octadecyloxy)benzene (PhC18) self-assembles to form a lamellar pattern (a = 2.7 ± 0.1 nm, b = 1.0 ± 0.1 nm, α = 85 ± 2°, Figure 6). The lamella width (~2.7 nm) is larger than that of a PhC10 SAMN (~1.8 nm), but is still smaller than the diameter of the coated AuNP (3.2 to 4 nm). Depositing a drop of an AuNP solution in tetradecane onto the PhC18-modified HOPG results in the adsorption of only a small number of AuNPs on top of the molecular template. At this low density of adsorption, the STM image (Figure 6d) clearly shows that AuNPs are preferentially centered on top of the aromatic units (bright features of the lamellae) of the SAMN.

The efficiency of AuNP templating by PhC18 was very low compared to PhC10 and PhC10-SAc SAMNs. Such a difference can be attributed to the mismatch between the length of the AuNP ligand (dodecanethiol) and the octadecyloxy chains of PhC18, which limits the vdW interactions between the particles transverse to the lamellae direction. Using AuNPs with the longer octadecanethiol (C18SH) ligand shell on the same PhC18 SAMN significantly increases the density of nanoparticle assemblies, albeit with limited long-range order (Figure SI13).

DISCUSSION

It is important to note that the self-assembly at the solid−liquid interface described here is very different from evaporation-driven crystallization reported for various (metal, semiconductor, polymer) nanoparticles.[45,46] The latter is defined exclusively by maximizing the interparticle interactions and thus produces close-packed hexagonal lattices. In contrast, the self-assembly at the liquid−solid interface is controlled by particle−surface interactions; it is generally self-limiting to a single monolayer and can produce other lattices. STM characterization under such conditions allows one to follow the dynamics of the AuNP assembly (Figures 2 and SI8) and to achieve high resolution on the underlying HOPG substrate, molecular templates, and AuNP superlattice.

The defining role of the molecular templates (SAMNs) is obvious from the fact that no ordered structures are obtained on HOPG in their absence. As seen from the low-coverage images (Figure 6), the AuNPs are centered preferentially on top of the aromatic rows of the SAMN, allowing AuNP alkyl chains to interact with the aliphatic lamellae, thereby maximizing vdW interactions. As a result, AuNPs assemble along the lamellae of the SAMN. When the periodicity of the SAMN matches the radius of the AuNP (including the ligands), an additional interaction arises from the vdW contacts of neighboring AuNP rows. This significantly increases the efficiency of self-assembly and large AuNP superlattices are formed on the surface, in an epitaxial relationship with the underlying template (*e.g.*, Figures 5 and SI7).

The presence of strongly binding functional groups in the SAMN (such as thiols) is not necessary for effective immobilization of AuNP and can actually be counterproductive in achieving highly ordered self-assembled structures. Indeed, acetylthiol-containing PhC10-SAc SAMNs yield a poorer quality of AuNP superlattices (smaller domains, more defects) compared to simple PhC10 SAMNs.

Figure 7 shows a schematic illustration of AuNP assembly on top of a SAMN, reflecting these observations. The center-to-center interparticle spacing (D_{nn}) between the AuNPs along the SAMN lamellae ($D_{nn}^{\parallel}$ = 3.1 ± 0.1 nm for PhC10-SAc and PhC10) is consistently shorter than that across the SAMN lamellae ($D_{nn}^{\perp}$ = 4.1 ± 0.1 nm for PhC10-SAc and 3.9 ± 0.1 nm for PhC10). Given that the metal core diameter of AuNP is 1.9 ± 0.3 nm (measured by TEM, Figure SI4), this yields a separation between the metal cores of $D_{cc}^{\parallel}$ ~1.2 nm and $D_{cc}^{\perp}$ ~2 nm, along and across the PhC10 lamellae,

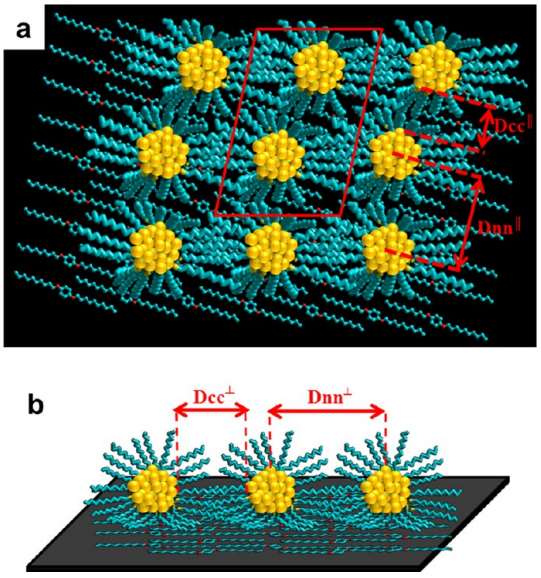

Figure 7. Schematic illustration of AuNP assembly on PhC10-modified HOPG from (a) top and (b) side view. D_{nn} and D_{cc} are the interparticle distances (center-to-center and core-to-core, respectively).

respectively. The derived thickness of the AuNP ligand shell along the lamellae (1/2 $D_{cc}^{\parallel}$ ~0.6 nm) is significantly smaller than the length of a fully extended dodecanethiol (L ~1.6 nm).[47] The thiol ligands must adopt some *gauche* conformations along the chain and bundle to enable such separation between the particles. This is expected considering the curved surface of AuNPs and is in good agreement with the shell thickness of 0.58 nm obtained from a molecular dynamics simulation of the monolayer of dodecanethiol-protected AuNPs on SAMN-free HOPG.[48] Across the lamellae the apparent thickness of the shell (1/2 $D_{cc}^{\perp}$ ~1.0 nm) is nearly twice as large but still is smaller than the length of the fully extended dodecanethiol ligand. This could be explained by a partial interdigitation of the fully extended ligand chains. The difference between the AuNP interactions in both directions is likely dictated by the asymmetry of the underlying SAMN template. Along the lamellae, the AuNP adopt a close-packed arrangement so as to maximize the interparticle vdW interactions. Transverse to the lamellae, the thiol ligands are most likely to be fully extended, which maximizes the vdW interactions with the alkyl chains of the template. The periodicity of the SAMN template controls the nanoparticle separation in the transverse direction ($D_{cc}^{\perp}$). When $D_{cc}^{\perp}$ matches the thickness of two (partially interpenetrated) AuNP ligand shells, the interparticle vdW interactions are maximized and stable well-ordered assemblies are obtained. Otherwise, more fluid, less dense, and thus less ordered assemblies can result. The former is manifested in C12SH-AuNPs on PhC10 templates (Figure 4), while the latter is observed for C12SH-AuNPs on PhC18 (Figure 5) and C8SH-AuNPs on PhC10 templates (Figure SI11).

CONCLUSION

In summary, we have demonstrated that periodic two-dimensional AuNP assemblies can be formed at the liquid−solid interface by prepatterning the surface (HOPG) with a self-assembled molecular network. The lamellar molecular adlayer acts as a sticky template, enabling the adsorption of AuNPs. Notably, the structural information of the monolayer is transferred to the AuNP assembly, which leads to superlattices with a non-centrosymmetric unit cell. This templating effect is primarily driven by van der Waals interactions between the alkyl chains of NP ligands and those of the underlying molecular template. When the length of the alkoxy chains of the molecular template matches that of the AuNP ligand, the enhanced particle−substrate and interparticle interactions lead to ordered assemblies that span hundreds of nanometers. When these conditions are not met, periodic assemblies of AuNP are not observed, despite the same chemical nature of the AuNP/SAMN interactions. Achieving the efficient 2D-templating effect at a solid−liquid interface thus creates a rational means to direct the self-organization of a variety of nanomaterials (metal nanoparticles, quantum dots, *etc.*) under dynamic equilibrium conditions. The resulting immobilization of AuNP in the ordered monolayer on HOPG enables high-resolution STM imaging of the internal structure of AuNPs in the liquid environment.

EXPERIMENTAL SECTION

Synthesis. *1,4-Di(decyloxy)benzene [PhC10].* A 1 L three-neck round-bottom flask was equipped with a stirring bar, a thermometer, a condenser, and a rubber septum and was flushed with Ar. 1-Bromodecane (72 mL, 0.35 mol), potassium iodide (5.86 g, 35.3 mmol), and potassium carbonate (50.9 g, 0.37 mol) were added to the solution of hydroquinone (15.1 g, 137 mmol) in Ar-purged DMF (220 mL). The reaction mixture was heated to 70 °C for 24 h under an argon atmosphere. After cooling to room temperature (results in the formation of a precipitate), distilled H_2O (500 mL) was added to the reaction mixture, and the solid material was isolated by filtration. Recrystallization from 2-propanol (800 mL) afforded colorless flakes of PhC10 (40.0 g, 75%), mp = 68−69 °C. ^{1}H NMR ($CDCl_3$): δ 6.82 (4H, s), 3.89 (4H, t, J = 6.5 Hz), 1.75 (4H, p, J = 7 Hz), 1.49−1.38 (4H, m), 1.38−1.21 (24H, m), 0.88 (6H, t, J = 7 Hz). ^{13}C NMR ($CDCl_3$): δ 153.16, 115.35, 68.64, 31.90, 29.60, 29.57, 29.43, 29.41, 29.33, 26.07, 22.69, 14.14.

1,4-Di(decyloxy)-2,5-bis(bromomethyl)benzene [PhC10-Br]. In a 250 mL one-neck round-bottom flask equipped with a stirring bar, 1,4-di(decyloxy)benzene (4.30 g, 11.0 mmol) and paraformaldehyde (1.008 g, 33.6 mmol) were suspended in glacial acetic acid (40 mL), followed by addition of 33 wt % hydrogen bromide solution in acetic acid (10 mL, 55 mmol). The flask was equipped with a condenser, and the reaction mixture was heated to 55 °C for 22 h under vigorous stirring. [*Note: a temperature increase above 70 °C results in formation of byproducts.*] The reaction

mixture was cooled to room temperature and poured into distilled H_2O. The solid material was collected by filtration, washed with H_2O to neutral pH, and dried under reduced pressure to afford PhC10-Br as a white powder (5.96 g, 94%), mp = 89−90 °C. ^{1}H NMR ($CDCl_3$): δ 6.85 (2H, s), 4.53 (4H, s), 3.98 (4H, t, J = 6.5 Hz), 1.81 (4H, p, J = 7 Hz), 1.56−1.43 (4H, m), 1.43−1.21 (24H, m), 0.88 (6H, t, J = 7 Hz). ^{13}C NMR ($CDCl_3$): δ 150.65, 127.50, 114.63, 69.00, 31.91, 29.60, 29.57, 29.37, 29.34, 28.78, 26.09, 22.69, 14.13.

1,4-Di(decyloxy)-2,5-bis(S-acetylthiomethyl)benzene [PhC10-SAc]. In a 250 mL one-neck round-bottom flask equipped with a stirring bar, potassium thioacetate (2.99 g, 26.1 mmol) was dissolved in DMF (70 mL), and 1,4-di(decyloxy)-2,5-bis-(bromomethyl)benzene (3.01 g, 5.22 mmol) was added to this solution. The reaction mixture was stirred at room temperature under nitrogen for 21 h. The suspension was poured into distilled H_2O, and the crude material was collected by filtration. Recrystallization from ethyl acetate (40 mL) afforded PhC10-SAc as a white cotton-like solid (2.50 g, 84%), mp = 78−79 °C. ^{1}H NMR ($CDCl_3$): δ 6.83 (2H, s), 4.08 (4H, s), 3.92 (4H, t, J = 6.5 Hz), 2.31 (6H, s), 1.75 (4H, p, J = 7 Hz), 1.51−1.39 (4H, m), 1.39−1.22 (24H, m), 0.88 (6H, t, J = 7 Hz). ^{13}C NMR ($CDCl_3$): δ 195.90, 150.36, 125.89, 114.00, 68.73, 31.92, 30.37, 29.62, 29.58, 29.39, 29.36, 28.55, 26.11, 22.70, 14.14. ESI$^+$ HRMS *m/z*: calcd for $C_{32}H_{54}O_4S_2$-Na 589.3356, found 589.3350 $(M + Na)^+$.

1,4-Di(decyloxy)-2,5-bis(hydrothiomethyl)benzene [PhC10-SH]. 1,4-Dioxane and distilled H_2O were degassed with bubbling nitrogen before use. In a 100 mL two-neck round-bottom flask equipped with a stirring bar, 1,4-di(decyloxy)-2,5-bis(*S*-acetylthiomethyl)-benzene (0.31 g, 0.54 mmol) was dissolved in 1,4-dioxane (22 mL). The flask was equipped with a condenser and a rubber septa, and the system was flushed with nitrogen. A 3.1 M aqueous solution of sodium hydroxide (0.7 mL, 2 mmol) was added dropwise to the above solution, and the reaction mixture was refluxed for 2 h. After cooling to room temperature, 2.0 M HCl (1.3 mL, 2.6 mmol) was added dropwise, and the mixture was stirred at rt for 1 h under N_2. H_2O was added, and the product was extracted into ethyl ether. The organic layer was washed with H_2O a few times and dried over $MgSO_4$ followed by filtration and solvent evaporation to give PhC10-SH as white powder (0.20 g, 76%). ^{1}H NMR: δ 6.78 (2H, s), 3.96 (4H, t, J = 6.5 Hz), 3.73 (4H, d, J = 7.8 Hz), 1.96 (2H, t, J = 8.1 Hz), 1.80 (4H, p, J = 7 Hz), 1.53−1.41 (4H, m), 1.41−1.22 (24H, m), 0.88 (6H, t, J = 6.5 Hz). ESI$^-$ HRMS *m/z*: calcd for $C_{28}H_{49}O_2S_2$ 481.3180, found 481.3183 $(M - H)^-$. [*Note: The product contains ca. 3% (by ^{1}H NMR) of disulfide dimer, which is also visible as a weak signal in the HRMS spectra: ESI$^-$ HRMS m/z calcd for $C_{56}H_{98}O_4S_4$ 961.6270, found 961.6298 $(M - H)^-$.*]

1,4-Di(octadecyloxy)benzene [PhC18]. This was synthesized following a similar procedure to that described for the synthesis of PhC10. A 1 L two-neck round-bottom flask was equipped with a stirring bar, a condenser, and a rubber septum and was flushed with N_2. Hydroquinone (6.66 g, 60.5 mmol), 1-bromooctadecane (48.60 g, 145.7 mmol), potassium carbonate (21.30 g 154.1 mmol), potassium iodide (2.17 g, 13.1 mmol), and Ar-purged DMF (250 mL) were mixed together and stirred at 55 °C for 3 days under a nitrogen atmosphere. After cooling to room temperature, distilled H_2O (600 mL) was added to the reaction mixture, and the solid material was isolated by filtration. To remove excess 1-bromooctadecane, the crude product was suspended in hot acetone and filtered. Recrystallization from 2-propanol (*ca.* 20 mL/g) afforded PhC18 as a light gray powder (26.80 g, 72%), mp = 88−89 °C. ^{1}H NMR ($CDCl_3$): δ 6.82 (4H, s), 3.89 (4H, t, J = 6.5 Hz), 1.75 (4H, p, J = 7 Hz), 1.50−1.20 (30H, m), 0.88 (6H, t, J = 7 Hz). ^{13}C NMR ($CDCl_3$): δ 153.17, 115.36, 68.65, 31.94, 29.71, 29.67, 29.62, 29.60, 29.44, 29.41, 29.38, 26.07, 22.71, 14.14.

Dodecanethiol-Protected Gold Nanoparticles (AuNP-C12SH). These were synthesized by the Brust−Schiffrin method described elsewhere.[35] Hydrogen tetrachloroaurate(III) trihydrate (0.050 g, 0.13 mmol) was dissolved in distilled water (8 mL) and then mixed with tetraoctylammonium bromide (0.382 g, 0.70 mmol) in toluene (25 mL). The mixture was stirred at room temperature for 30 min to facilitate the phase transfer of the $AuCl_4^-$ into the toluene layer. The aqueous layer was then discarded. The organic layer was cooled to 0 °C. Dodecanethiol (0.077 g, 0.39 mmol) was added to the solution *via* a micropipet and allowed to stir for 10 min. A fresh solution of sodium borohydride (0.055 g, 1.45 mmol) in water (8 mL) was added to the rapidly stirring reaction mixture over 5 s. The color of the solution became dark red instantly. The mixture was allowed to warm to room temperature and left under stirring overnight (~18 h). The aqueous layer was removed, and the toluene layer was washed with distilled water (3 × 20 mL) and dried over $MgSO_4$, followed by filtration and solvent removal under reduced pressure. Crude AuNPs were suspended in 50 mL of 95% ethanol and placed in a freezer overnight. The supernatant was decanted, and the AuNP precipitate was washed with 95% ethanol (10 × 15 mL). The average size of obtained AuNPs is 1.9 ± 0.3 nm (see Figure S4).

STM Imaging. All STM experiments were performed using a Digital Instruments Inc. (Veeco) NanoScope V. The STM tips were mechanically cut from Pt/Ir wire (80/20, diameter 0.25 mm, Nanoscience). PhC10-SAc, PhC10-SH, PhC10, and PhC18 molecules and AuNPs were dissolved in tetradecane (Sigma-Aldrich, ≥99.8%) and used directly without further purification. The physisorbed monolayer was formed spontaneously after deposition of 10 to 15 μL of saturated solutions onto freshly cleaved HOPG (grade SPI-2, SPI Supplies). The nanoparticle superlattice was formed at the liquid−solid interface by applying a volume of 10 to 15 μL of AuNP solution onto the organic monolayer modified HOPG. The experimental time (1−3 h) was always shorter than the evaporation of solvent from HOPG (>10 h; bp of tetradecane is 252−254 °C).

All STM images were obtained in the constant current mode by applying a tunneling current I_{set} of 70 to 250 pA and a sample bias V_{set} of 500 to 1400 mV. The raw images were processed from WSxM5.0 and SPIP 6.0.3 software. The calibration of the STM images of the molecular networks was performed through 2D-FFT using the underlying graphite lattice unit cell. The drift in images of the AuNP assembly was minimized by a repetitive scanning up and down until the unit cell parameters became independent of the scanning directions.

Molecular Modeling. The geometry optimizations of the molecular networks of PhC10-SAc, PhC10, and PhC18 were performed using HyperChem 8.0 software (from Hypercube Inc.), applying the MM+ force field with the Polak−Ribiere gradient optimization algorithm and a root-mean-square gradient convergence criterion of 0.001 kcal Å^{-1} mol^{-1}.

PhC10-SAc, PhC10, and PhC18 assemblies on graphite were simulated using a single layer of graphene covered with a monolayer of 16 molecules. Assemblies of PhC10-SAc, PhC10, and PhC18 molecules were placed on the graphene sheet, in geometries approximating the observed unit cell, and allowed to fully relax (while the graphene atom positions were fully constrained).

Conflict of Interest: The authors declare no competing financial interest.

Acknowledgment. This work was supported by NSERC Discovery Grants (Canada) and a FQRNT Team Grant (Quebec). M.A. M. thanks NSERC and FQRNT for the doctoral fellowships. I.I.P. acknowledges FQRNT for the postdoctoral fellowship.

Supporting Information Available: ^{1}H and ^{13}C NMR of PhC10, PhC10-Br, PhC10-SAc, PhC10-SH, PhC18; TEM of AuNP; synthesis of PhC10-SH; additional STM images. This material is available free of charge *via* the Internet at http://pubs.acs.org.

REFERENCES AND NOTES

1. Nie, Z.; Petukhova, A.; Kumacheva, E. Properties and Emerging Applications of Self-assembled Structures Made from Inorganic Nanoparticles. *Nat. Nanotechnol.* **2010**, *5*, 15–25.
2. Piner, R. D.; Zhu, J.; Xu, F.; Hong, S.; Mirkin, C. A. Dip-Pen Nanolithography. *Science* **1999**, *283*, 661–663.
3. Liu, S.; Maoz, R.; Sagiv, J. Planned Nanostructures of Colloidal Gold *via* Self-assembly on Hierarchically Assembled Organic Bilayer Template Patterns with *in-situ* Generated Terminal Amino Functionality. *Nano Lett.* **2004**, *4*, 845–851.
4. Whitesides, G. M.; Grzybowski, B. Self-assembly at All Scales. *Science* **2002**, *295*, 2418–2421.

5. Hamley, I. W. Nanotechnology with Soft Materials. *Angew. Chem., Int. Ed.* **2003**, *42*, 1692–1712.
6. Lei, Y.; Yang, S.; Wu, M.; Wilde, G. Surface Patterning Using Templates: Concept, Properties and Device Applications. *Chem. Soc. Rev.* **2011**, *40*, 1247–1258.
7. De Feyter, S.; De Schryver, F. C. Two-dimensional Supramolecular Self-Assembly Probed by Scanning Tunneling Microscopy. *Chem. Soc. Rev.* **2003**, *32*, 139–150.
8. Ciesielski, A.; Palma, C.-A.; Bonini, M.; Samori, P. Towards Supramolecular Engineering of Functional Nanomaterials: Pre-Programming Multi-Component 2D Self-Assembly at Solid−Liquid Interfaces. *Adv. Mater.* **2010**, *22*, 3506–3520.
9. Mena-Osteritz, E.; Bäuerle, P. Complexation of C60 on a Cyclothiophene Monolayer Template. *Adv. Mater.* **2006**, *18*, 447–451.
10. Li, M.; Deng, K.; Lei, S. B.; Yang, Y. L.; Wang, T. S.; Shen, Y. T.; Wang, C. R.; Zeng, Q. D.; Wang, C. Site-selective Fabrication of Two-Dimensional Fullerene Arrays by Using a Supramolecular Template at the Liquid−Solid Interface. *Angew. Chem., Int. Ed.* **2008**, *47*, 6717–6721.
11. MacLeod, J. M.; Ivasenko, O.; Fu, C.; Taerum, T.; Rosei, F.; Perepichka, D. F. Supramolecular Ordering in Oligothiophene−Fullerene Monolayers. *J. Am. Chem. Soc.* **2009**, *131*, 16844–16850.
12. Griessl, S. J. H.; Lackinger, M.; Jamitzky, F.; Markert, T.; Hietschold, M.; Heckl, W. M. Incorporation and Manipulation of Coronene in an Organic Template Structure. *Langmuir* **2004**, *20*, 9403–9407.
13. Schull, G.; Douillard, L.; Fiorini-Debuisschert, C.; Charra, F.; Mathevet, F.; Kreher, D.; Attias, A. J. Single-molecule Dynamics in a Self-Assembled 2D Molecular Sieve. *Nano Lett.* **2006**, *6*, 1360–1363.
14. Adisoejoso, J.; Tahara, K.; Okuhata, S.; Lei, S.; Tobe, Y.; De Feyter, S. Two-Dimensional Crystal Engineering: A Four-Component Architecture at a Liquid−Solid Interface. *Angew. Chem., Int. Ed.* **2009**, *48*, 7353–7357.
15. Lu, J.; Lei, S. B.; Zeng, Q. D.; Kang, S. Z.; Wang, C.; Wan, L. J.; Bai, C. L. Template-Induced Inclusion Structures with Copper (II) Phthalocyanine and Coronene as Guests in Two-Dimensional Hydrogen-Bonded Host Networks. *J. Phys. Chem. B* **2004**, *108*, 5161–5165.
16. Ivasenko, O.; MacLeod, J. M.; Chernichenko, K. Yu.; Balenkova, E. S.; Shpanchenko, R. V.; Nenajdenko, V. G.; Rosei, F.; Perepichka, D. F. Supramolecular Assembly of Heterocirculenes in 2D and 3D. *Chem. Commun.* **2009**, 1192–1194.
17. Den Boer, D.; Habets, T.; Coenen, M. J. J.; Van Der Maas, M.; Peters, T. P. J.; Crossley, M. J.; Khoury, T.; Rowan, A. E.; Nolte, R. J. M.; Speller, S.; Elemans, J. A. A. W. Controlled Templating of Porphyrins by a Molecular Command Layer. *Langmuir* **2011**, *27*, 2644–2651.
18. Daniel, M. C.; Astruc, D. Gold Nanoparticles: Assembly, Supramolecular Chemistry, Quantum-Size-Related Properties, and Applications toward Biology, Catalysis, and Nanotechnology. *Chem. Rev.* **2004**, *104*, 293–346.
19. Pelaz, B.; Jaber, S.; De Aberasturi, D. J.; Wulf, V.; Aida, T.; De La Fuente, J. M.; Feldmann, J.; Gaub, H. E.; Josephson, L.; Kagan, C. R.; Kotov, N. A.; Liz-Marzán, L. M.; Mattoussi, H.; Mulvaney, P.; Murray, C. B.; Rogach, A. L.; Weiss, P. S.; Willner, I.; Parak, W. J. The State of Nanoparticle-Based Nanoscience and Biotechnology: Progress, Promises, and Challenges. *ACS Nano* **2012**, *6*, 8468–8483.
20. Acharya, S.; Hill, J. P.; Ariga, K. Soft Langmuir-Blodgett Technique for Hard Nanomaterials. *Adv. Mater.* **2009**, *21*, 2959–2981.
21. Rao, C. N. R.; Kalyanikutty, K. P. The Liquid−Liquid Interface as a Medium to Generate Nanocrystalline Films of Inorganic Materials. *Acc. Chem. Res.* **2008**, *41*, 489–499.
22. Bigioni, T. P.; Lin, X.-M.; Nguyen, T. T.; Corwin, E. I.; Witten, T. A.; Jaeger, H. M. Kinetically Driven Self Assembly of Highly Ordered Nanoparticle Monolayers. *Nat. Mater.* **2006**, *5*, 265–270.
23. Aldaye, F. A.; Palmer, A. L.; Sleiman, H. F. Assembling Materials with DNA as the Guide. *Science* **2008**, *321*, 1795–1799.
24. Shenhar, R.; Norsten, T. B.; Rotello, V. M. Polymer-Mediated Nanoparticles Assembly: Structural Control and Applications. *Adv. Mater.* **2005**, *17*, 657–669.
25. Chiu, J. J.; Kim, B. J.; Kramer, E. J.; Pine, D. J. Control of Nanoparticle Location in Block Copolymers. *J. Am. Chem. Soc.* **2005**, *127*, 5036–5037.
26. Perepichka, I. I.; Ximin, C.; Bazuin, C. G. Nanopatterning of Substrates by Self-Assembly in Supramolecular Block Copolymer Monolayer Films. *Sci. China, Chem.* **2013**, *56*, 48–55.
27. Hoeppener, S.; Chi, L.; Fuchs, H. Formation of Au55 Strands on a Molecular Template at the Solid−Liquid Interface. *Nano Lett.* **2002**, *2*, 459–463.
28. Lei, S. B.; Wang, C.; Yin, S. X.; Wan, L. J.; Bai, C. L. Assembling Nanometer Nickel Particles into Ordered Arrays. *Chem. Phys. Chem.* **2003**, *4*, 1114–1117.
29. Wei, X.; Tong, W.; Fidler, V.; Zimmt, M. B. Reactive Capture of Gold Nanoparticles by Strongly Physisorbed Monolayers on Graphite. *J. Colloid Interface Sci.* **2012**, *387*, 221–227.
30. Hansen, T.; Itoua, S.; Kamounah, F. S.; Christensen, J. B.; Bjørnholm, T.; Schaumburg, K.; Bechgaard, K.; Wilkes, S. B. STM Investigations of Physisorbed Monolayers of Dialkoxy-Substituted Aromatics. *J. Mater. Chem.* **1999**, *9*, 1107–1113.
31. Shao, X.; Luo, X.; Hu, X.; Wu, K. Solvent Effect on Self-Assembled Structures of 3,8-Bis-Hexadecyloxy-Benzo-[*c*]Cinnoline on Highly Oriented Pyrolytic Graphite. *J. Phys. Chem. B* **2006**, *110*, 1288–1293.
32. Wei, Y.; Tong, W.; Zimmt, M. B. Self-Assembly of Patterned Monolayers with Nanometer Features: Molecular Selection Based on Dipole Interactions and Chain Length. *J. Am. Chem. Soc.* **2008**, *130*, 3399–3405.
33. Tour, J. M.; Jones, L., II; Pearson, D. L.; Lamba, J. J. S.; Burgin, T. P.; Whitesides, G. M.; Allara, D. L.; Parikh, A. N.; Atre, S. Self-Assembled Monolayers and Multilayers of Conjugated Thiols, Alpha,Omega-Dithiols, and Thioacetyl-Containing Adsorbates. Understanding Attachments between Potential Molecular Wires and Gold Surfaces. *J. Am. Chem. Soc.* **1995**, *117*, 9529–9534.
34. Elemans, J. A. A. W.; de Cat, I.; Xu, H.; de Feyter, S. Two-Dimensional Chirality at Liquid−Solid Interfaces. *Chem. Soc. Rev.* **2009**, *38*, 722–736.
35. Brust, M.; Walker, M.; Bethell, D.; Schiffrin, D. J.; Whyman, R. J. Synthesis of Thiol-Derivatized Gold Nanoparticles in a Two-Phase Liquid−Liquid System. *J. Chem. Soc., Chem. Commun.* **1994**, 801–802.
36. Auer, S.; Frenkel, D. Suppression of Crystal Nucleation in Polydisperse Colloids due to Increase of the Surface Free Energy. *Nature* **2001**, *413*, 711–713.
37. Grumelli, D.; Vericat, C.; Benitez, G.; Vela, M. E.; Salvarezza, R. C.; Giovanetti, L. J.; Ramallo-Lopez, J. M.; Requejo, F. G.; Craievich, A. F.; Shon, Y. S. Thiol-Capped Gold Nanoparticles on Graphite: Spontaneous Adsorption and Electrochemically Induced Release. *J. Phys. Chem. C* **2007**, *111*, 7179–7184.
38. Orive, A. G.; Grumelli, D.; Vericat, C.; Ramallo-López, J. M.; Giovanetti, L.; Benitez, G.; Azcárate, J. C.; Corthey, G.; Fonticelli, M. H.; Requejo, F. G.; Hernández Creus, A.; Salvarezza, R. C. "Naked" Gold Nanoparticles Supported on HOPG: Melanin Functionalization and Catalytic Activity. *Nanoscale* **2011**, *3*, 1708–1716.
39. Talapin, D. V.; Shevchenko, E. V.; Murray, C. B.; Titov, A. V.; Kral, P. Dipole−Dipole Interactions in Nanoparticle Superlattices. *Nano Lett.* **2007**, *7*, 1213–1219.
40. Prasad, B. L. V.; Sorensen, C. M.; Klabunde, K. J. Gold Nanoparticle Superlattices. *Chem. Soc. Rev.* **2008**, *37*, 1871–1883.
41. Jackson, A. M.; Hu, Y.; Silva, P. J.; Stellacci, F. From Homoligand- to Mixed-Ligand Monolayer-Protected Metal Nanoparticles: A Scanning Tunneling Microscopy Investigation. *J. Am. Chem. Soc.* **2006**, *128*, 11135–11149.
42. Ong, Q. K.; Reguera, J.; Silva, P. J.; Moglianetti, M.; Harkness, K.; Longobardi, M.; Mali, K. S.; Renner, C.; De Feyter, S.; Stellacci, F. High-Resolution Scanning Tunneling Microscopy Characterization of Mixed Monolayer Protected Gold Nanoparticles. *ACS Nano* **2013**, *7*, 8529–8539.

43. Cesbron, Y.; Shaw, C. P.; Birchall, J. P.; Free, P.; Lévy, R. Stripy Nanoparticles Revisited. *Small* **2012**, *8*, 3714–3719.
44. Yu, M.; Stellacci, F. Response to "Stripy Nanoparticles Revisited". *Small* **2012**, *8*, 3720–3726.
45. Claridge, S. A.; Castleman, A. W.; Khanna, S. N.; Murray, C. B.; Sen, A.; Weiss, P. S. Cluster-Assembled Materials. *ACS Nano* **2009**, *3*, 244–255.
46. Nie, Z.; Petukhova, A.; Kumacheva, E. Properties and Emerging Applications of Self-Assembled Structures Made from Inorganic Nanoparticles. *Nat. Nanotechnol.* **2010**, *5*, 15–25.
47. Whetten, R. L.; Shafigullin, M. N.; Khoury, J. T.; Schaaff, T. G.; Vezmar, I.; Alvarez, M. M.; Wilkinson, A. Crystal Structures of Molecular Gold Nanocrystal Arrays. *Acc. Chem. Res.* **1999**, *32*, 397–406.
48. Luedtke, W. D.; Landman, U. Structure, Dynamics, and Thermodynamics of Passivated Gold Nanocrystallites and Their Assemblies. *J. Phys. Chem.* **1996**, *100*, 13323–13329.